SECOND INTERNATIONAL CONFERENCE ON
PORT AND OCEAN ENGINEERING UNDER ARCTIC CONDITIONS
UNIVERSITY OF ICELAND
DEPARTMENT OF ENGINEERING AND SCIENCE

THE DEFORMATION OF AN ARCTIC ICE ISLAND

G. Holdsworth — Department of the Environment — Ottawa, Canada
A. Traetteberg — River and Harbour Laboratory — Trondheim, Norway

ABSTRACT

An experiment is described in which a laser interferometer was used to measure the strain rate on the surface of Fletcher's Ice Island T 3, which is a drifting slab of shelf ice averaging 30 m thick and measuring 6 km by 11 km. The island is currently less than 100 km off the north-west coast of Ellesmere Island, and during most of the time of the experiment, it appeared to be gripped in the pack ice. According to Weertman's creep theory[1] the maximum "effective shear stress" is 0.010 MN m^{-2} at the site of the laser experiment. Using current flow law data and some field measurements from Ward-Hunt Ice Shelf, the expected creep rate corresponding to this stress acting within the ice at an average temperature of -8.3°C is in the range 3×10^{-12} to 3×10^{-11} s^{-1}. The preliminary strain rate data obtained over 50 and 100 m line lengths indicates that predominantly compressive stresses were acting in the general direction of the line throughout the measurements. The compressive strain rates were of order 10^{-11} to 10^{-10} s^{-1}. Superimposed on the compression were cyclical strain oscillations, one of which had an average period of about 35 s. This was close to the average period of beam swing (37 s) of a gravity meter mounted near the edge of the island. These observations are consistent with the existence of flexural waves in the island.

INTRODUCTION

Fletcher's Ice Island T 3 is a drifting fragment of a former N.W. Ellesmere Island ice shelf. It was first sighted in 1947 and occupied by the U.S.A.F. since 1952. At that time it measured 17 x 8 km and was up to 60 m thick in some places. It now averages 30 m thick and measures 11 x 6 km. At the time of the experiment, it was situated between 82° 40' - 82° 46' latitude and 85° - 86° longitude and appeared to be gripped in the pack ice (Fig. 1).

The present work was done between the 16th of April and the 26th of May,

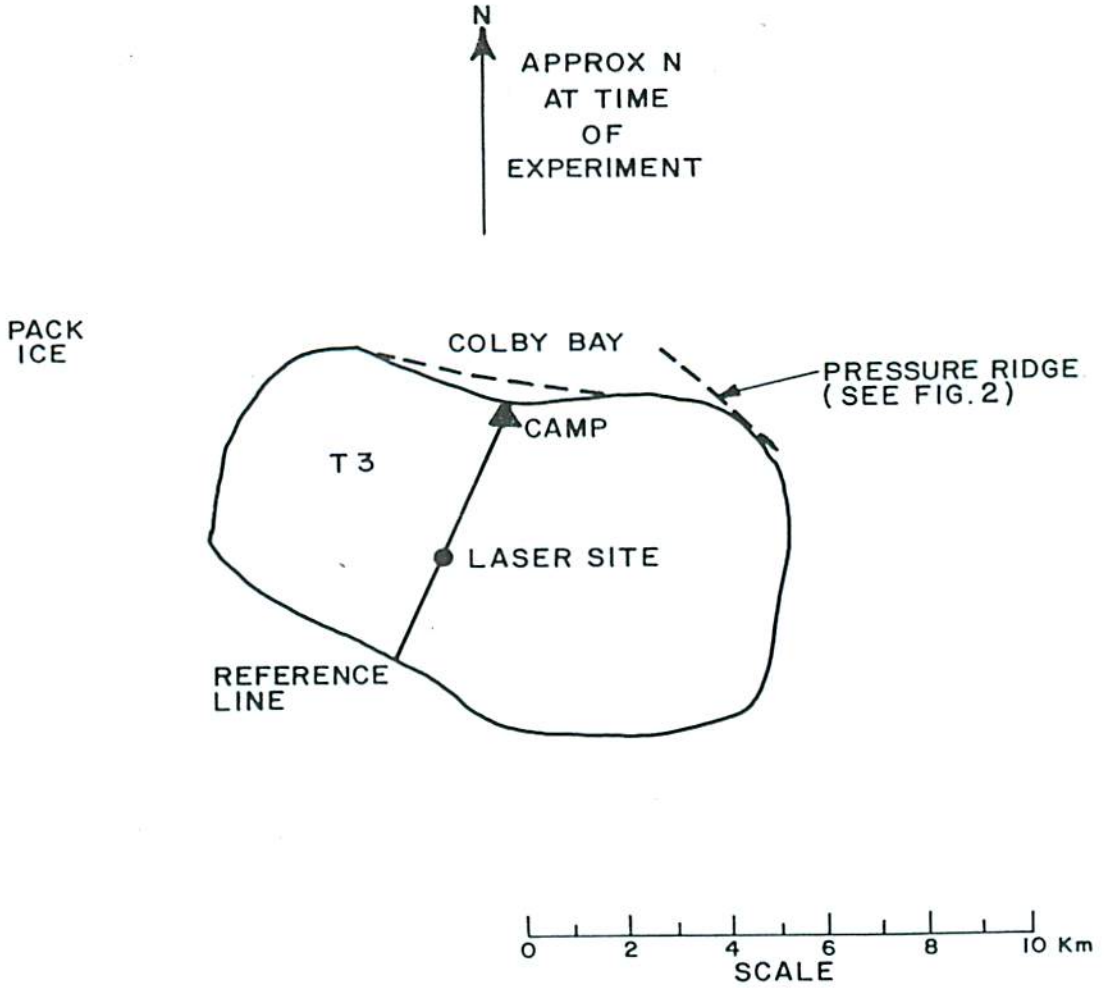

Fig. 1. Ice Island T 3 showing approximate shape and orientation at time of experiment.

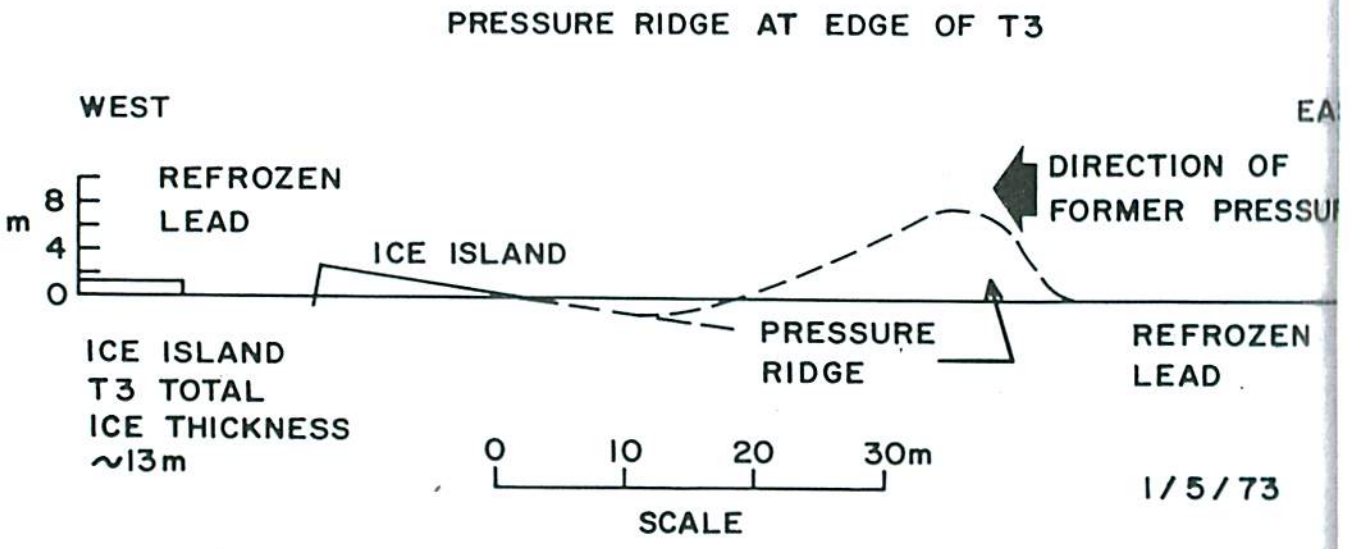

Fig. 2. Cross-section of pressure ridge on edge of island, May 1. Ridge formed April 30 - May 1, 1973.

1973, at which time the surface was covered by about 0.4 - 0.5 m of winter snow and no melt water was present.

No previous measurements of strain rate on the island have been reported, although some attempts have been made (Hunkins, personal communication).

The average movement for the latter half of April and up to the 19th of May was about 0.5 km day^{-1}. During a storm from May 20-22, the island was displaced over 12 km, after which the movements returned substantially to the previous rates. It appears that in moving with the pack ice, and in convergent conditions, pieces of the edge of the island may be broken off due to thrusting of pressure ridges up onto the island (Fig. 2). This seems to be the main cause of (areal) size reduction of the island. Net surface ablation rates[2] are of order 0.5 - 1 m. a^{-1} whereas bottom melting is probably much less. Compressive horizontal strains are interpreted as being caused by pack ice thrust and thermal strains by cooling. Extensive horizontal strains are interpreted as being caused by Weertman creep[1] and thermal strains due to warming. The magnitude of these net strains appears to lie between 10^{-12} and 10^{-10} s^{-1} and any one component might not act continuously. Under divergent conditions and temperature increase the island will expand horizontally; under convergent conditions with cooling it will contract. Under various other combinations of these conditions, the determination of behaviour requires rigorous measurements.

With the recent developments in laser metrology, it is now possible to measure displacements between two points about 100 m apart, in an 8 hour working day, when the <u>average</u> strain rate is between 10^{-11} and 10^{-10} s^{-1}. This has been done using a Hewlett Packard laser interferometer.

INSTRUMENTATION

The system used consisted of the following Hewlett Packard units:

1, 5505A laser display unit;
1, 5500C laser head with tripod;
1, 10565B remote interferometer;
1, 10550B reflector and mount.

Principle Of Operation (modified from Hewlett Packard Manual No. 05526-90001).

The laser head consists of a low power Helium-Neon, 2 frequency laser with automatic tuning and instant warm up capabilities. The two different frequencies are of opposite circular polarization. The experiment used an external remote interferometer and reflector. The beam exiting from the laser head is split at the surface of a polarizing beam splitter, with one (reference) frequency reflected from the reference corner cube mounted on the housing of the interferometer. The other frequency is transmitted to the reflector, and returns, to be passed with the reference frequency back along a common axis through a demodulating polarizer to the photodetector block in the laser head.

Relative motions between the interferometer cube and the reflector cause a difference in the Doppler shifts in the frequencies of the returning beam. The difference between the frequency registered by the measurement photodetector and the frequency registered by the reference photodetector is monitored by a subtractor and accumulated in a fringe-count register. A digital calculator samples the accumulated value every 5 ms and performs a two-stage multiplication: one for refractive index correction and the other for conversion to inches or mm. The display shows, on selection, either distance or velocity. The distance shown on the laser display at any time is equal to the product of the laser (air) wavelength x the number of wavelengths of motion counted since the reset button was last pressed. The ratio of $\frac{\text{air wavelength}}{\text{vacuum wavelength}}$ is used in the calculation and for normal conditions of use the value is 0.999,XXX,X where the last four places are determined from the temperature, pressure and humidity of the air. Neither the automatic compensator (model 5510A) nor the compensation tables covered the appropriate range of conditions, therefore it was decided to leave an arbitrary value of XXX,X set in the instrument (by thumbwheel switch control) and correct for the change in pressure, temperature and humidity later. It turned out that this correction was negligible when rounding off readings to the 4th decimal place of mm. The stated accuracy is ±0.5 ppm ±2 counts in the last digit; resolution in smooth or normal modes is 0.0001, in x 10 mode, 0.00001 mm.

The reset signal is triggered (1) by beam interruption (< 5% of beam returned), (2) when there is a tuning error, or (3) when the maximum allowable measuring velocity (0.3 m. s^{-1}) is exceeded. Rather than use a digital recorder, it was decided to manually record the readings from the display because of the (periodically) high rate of reset and the general lack of requirement for very closely spaced data. Furthermore, the necessity for occasional re-alignment of the beam and of reading the pressure, and temperature and ensuring a steady flow of air through the laser box, required an operator to be present.

Operation Of The System

The final arrangement is shown in Figures 3 and 4. To ensure stability of the laser, the tripod was mounted on the ice through holes in the floor of the operating hut. The feet of the tripod were frozen into shallow holes in the ice. The laser head and tripod were surrounded by a lagged box, the inside temperature of which was maintained at approximately the same value as in the tunnel. Access to the interior was gained by a side door. The remote interferometer was mounted on an adjustable post consisting of a 10 cm diameter, 4 m long tube, $3\frac{1}{2}$ m of which was frozen into the ice. Inside this tube was fitted a 2 m long sliding tube, on top of which was mounted a plate. The tube could be clamped at any level by a rod and cone system and locked by a knurled

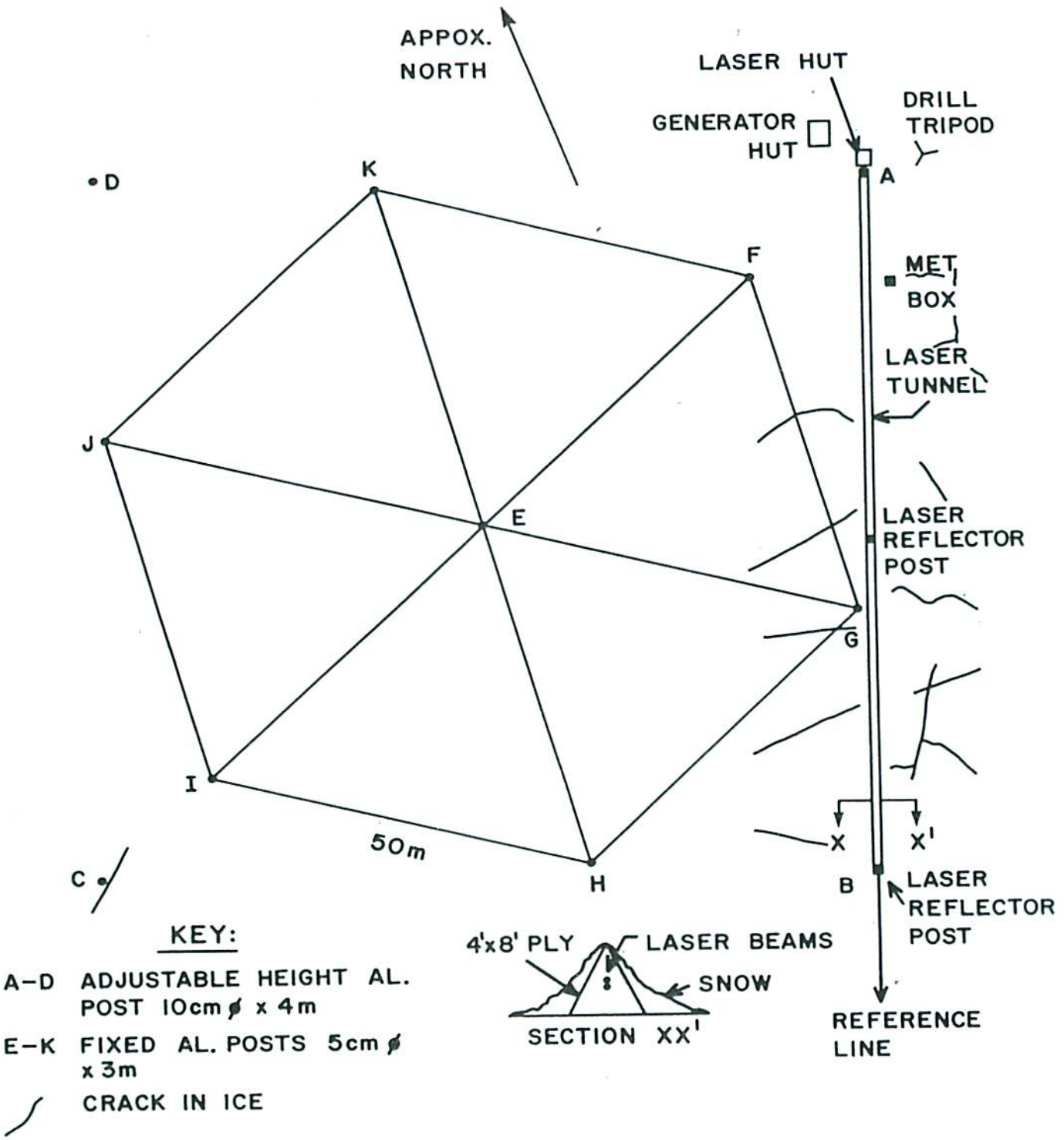

Fig. 3. Plan view of laser experiment site, showing installations.

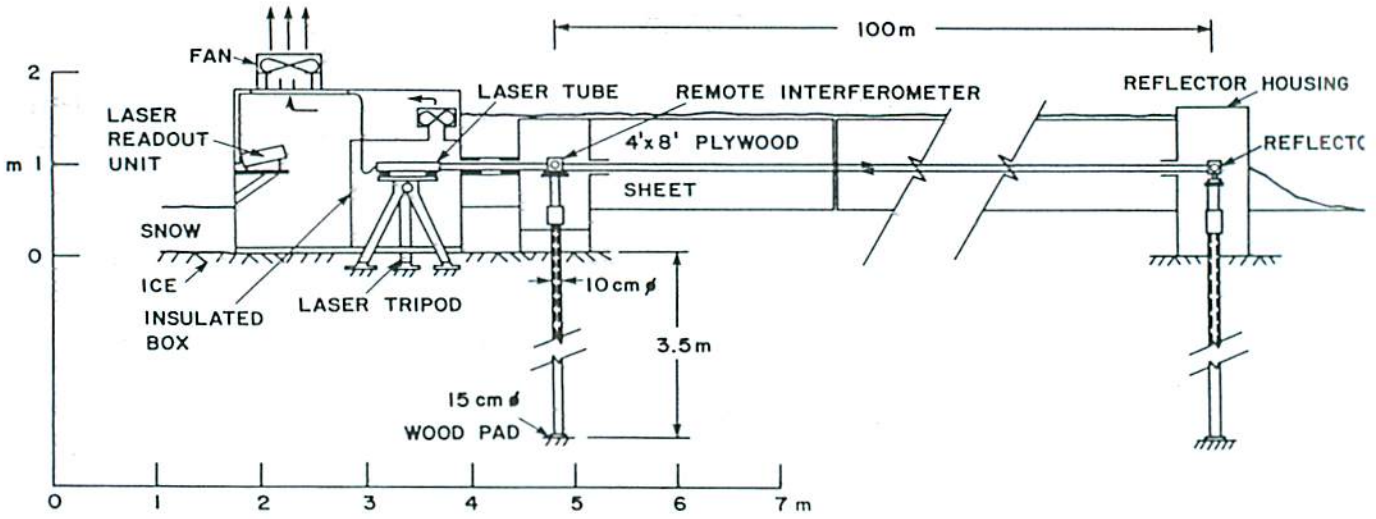

Fig. 4. Cross-section through laser interferometer instrumentation.

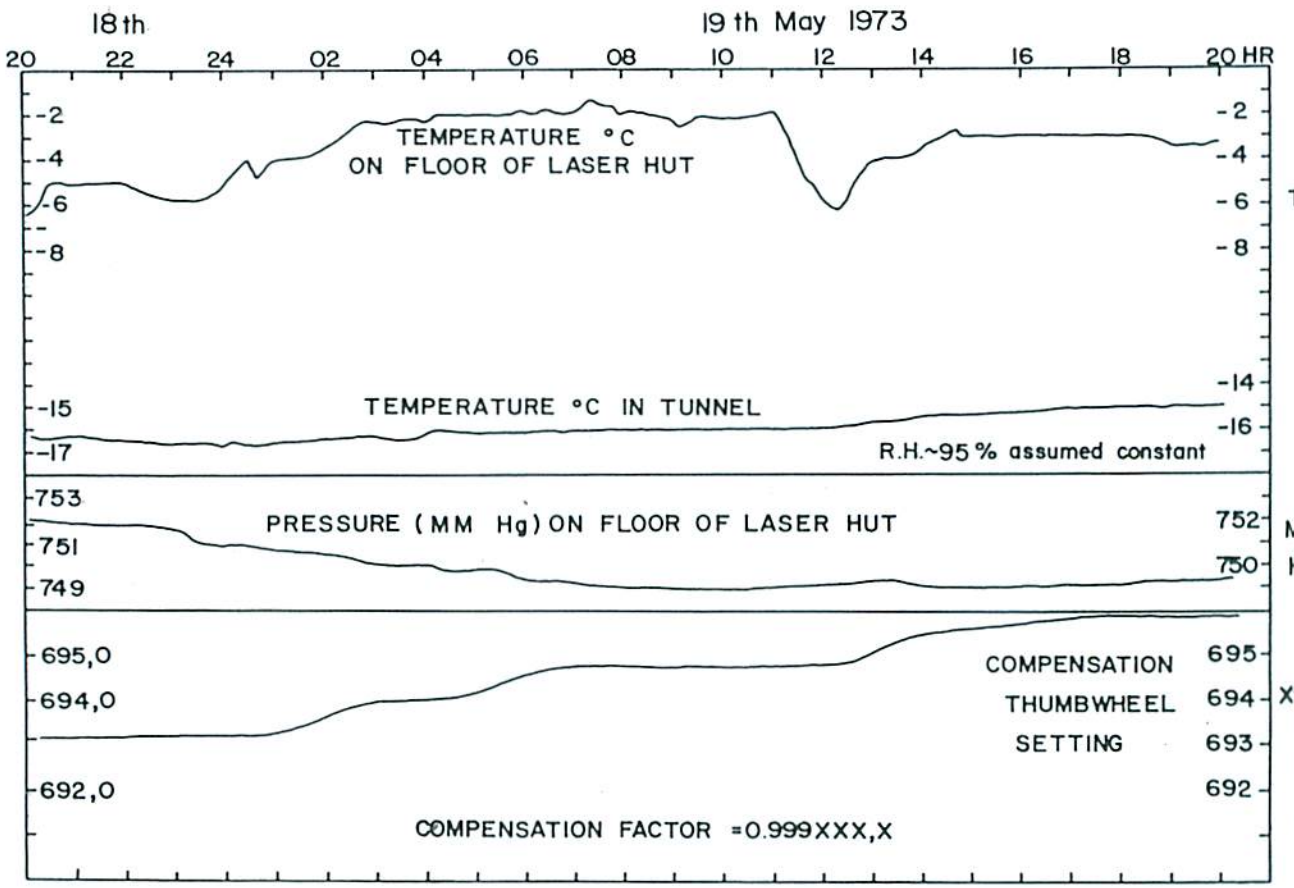

Fig. 5. Plot of temperature, pressure and compensation factor variations with time for the 24 hour laser run.

ring. The reflector was mounted on a similar post at distances of 52.85 m and 99.76 m from the remote interferometer. The laser hut, remote interferometer, and reflector housing were all linked by a tunnel made from 44 pairs of connected 4' x 8' plywood sheets set in the shape of an A-frame and covered by snow to reduce radiation heating inside the tunnel and stabilize temperatures along the path of the laser beam. The tunnel had the effect of sustaining a draft through the laser box if there was a slight wind. In addition, the tunnel allowed the experiment to be run under adverse weather conditions.

The beam alignment was achieved by trial and error before the completion of the laser box and tunnel. Any further adjustments were made either by rotating the rear levelling thumb screw of the laser head, or by slight repositioning of the interferometer and/or the reflector. Severe flutter of the return beam at the entrance port to the laser head was the only apparent problem. When less than 5% of the return beam was intercepted the reset warning would be triggered, and the display reading would return to zero. As a result, the longest period of operation without a reset was about 4 hours. A system of fans was installed to induce draft when the wind was insufficient to maintain a steady flow of air through the tunnel, laser box and hut. This was necessary to prevent excessive beam flutter due to strong temperature gradients in front of the laser head. After switch on a period would usually be allowed to elapse until the system stabilized. Beam flutter was prevented (for limited periods of time) by adjusting the forced draft and waiting until the box temperature was close to the tunnel temperature.

For the longer measurement runs, display readings would be taken every minute, temperature and pressure every 10 minutes. Humidity was automatically recorded in a meteorological screen and was mostly between 90-100%, (Appendix).

Several shorter runs were made. Over a period of an hour readings were recorded about every second, simultaneously with gravimeter measurements taken near the north edge of the island. Generally, with the successful runs, the beam alignment meter (indicating strength of signal) would normally indicate 7 ± 0.5 whereas the cutoff signal strength for reset is 4.0. Since resets could occur even with this relatively high signal strength, it was deduced that there occurred large fluctuations in the signal of higher frequency than the meter could respond to. The possibility of pulses of strain produced by pack ice interaction with the island remains open to question.

RESULTS

A 24 hour run was made using the 99.76 m line, from May 18, 2000 hrs to May 19, 2000 hrs. Figure 5 shows the values of temperature, pressure and humidity as well as the compensation thumbwheel setting XXX,X at ten minute intervals. The corrected distance d' is calculated from:

$$d' = d \times \frac{0.999XXX,X}{0.999725,0}$$

where d is the distance read off the instrument and the digits 725,0 were arbitrarily left in the instrument. Figure 6 shows the corrected time-displacement plot where each point represents a ten minute mean. The reset points have been joined using separate plots of differences between readings versus time and interpolating to the reset time. The smaller fluctuations are filtered out. There appears to be an oscillation of average period 1 hour. This may be due to wave motion[3] causing flexure of the ice and hence alternate compression and extension as will be shown for the case where the period of oscillation is about 35 s. Nevertheless, there is net compression when averaging is done over times greater than about 4 hours. The average strain rate is about -2.64×10^{-11} s^{-1}. Figure 7 shows two other runs of shorter duration (4 hours), along the same line but for a distance of 52.85 m. As before, the averaging has been done over intervals of 10 minutes and it can be seen that an oscillation of period about 1 hour is still evident. The apparent net compression is again in accordance with the observed boundary conditions. Both Figure 6 and 7 show compressive strain rates which are composed of a strain rate of mechanical origin and one of thermal origin. As a result of clock calibration, times must be reduced by 1.6% in order to obtain correct strain rates.

ADDITIONAL STRAIN MEASUREMENTS

An hexagonal strain net was established (Fig. 3) consisting of 7, 2"(5.08 cm) diameter, 10'(3 m) long capped aluminum tubes resting on a 6"(15 cm) wooden base plate and frozen into the ice in a vertical position. The tubes were all installed by April 25. Because of the freezing-in process, a thermistor line was installed beside one of the tubes (K - Fig. 3) and the temperature was monitored until the ice temperature had returned essentially to its former value. This occupied about 1 week. Taping measurements were made on May 1, 14, and 24.

The tubes had been installed so that the taping spikes mounted on the upper caps were all level. Because of variations in the elevation of the ice surface (Fig. 8), tube lengths above the snow level varied from about 0.5 to 1 m. This was done so that all lines were horizontal. Each side, of length 50 m ± 0.07 m was measured with a calibrated 50 m K and E Lovar tape supported at mid-span. At either end, Kern tension frames - modified to be self-supporting - were used. The weights were 15 Kg each. The tape was read at both ends using a reader band. A minimum of three readings were taken at each end until the spread in readings was within 0.2 mm, although individual readings were estimated to 0.1 mm. Distances were corrected for air (tape) temperature.

The measurements were made initially without shading the tubes which,

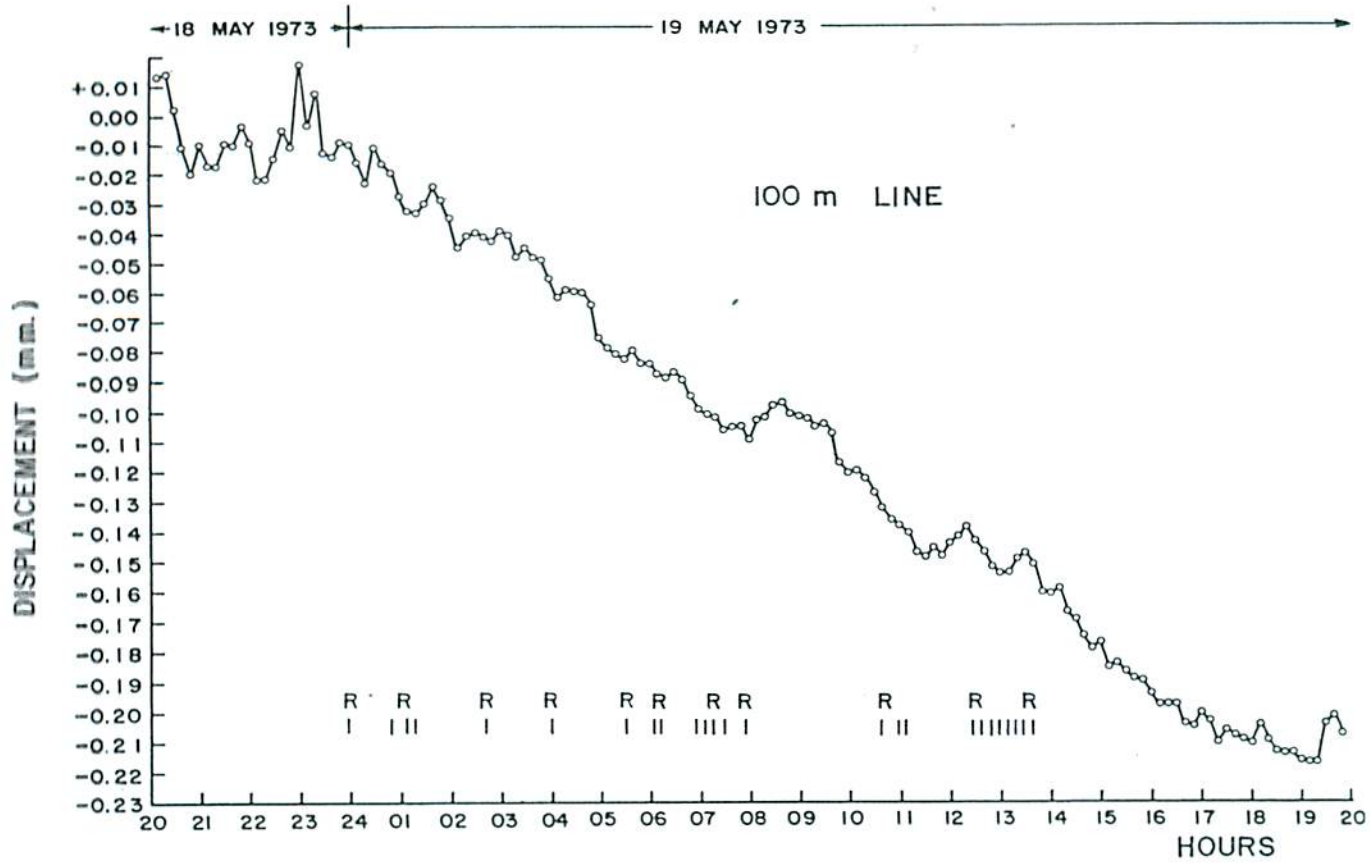

Fig. 6. Time-displacement plot for the 100 m line, May 18-19, 1973. Places marked by R are reset points. The average strain rate is -2.64×10^{-11} s^{-1}.

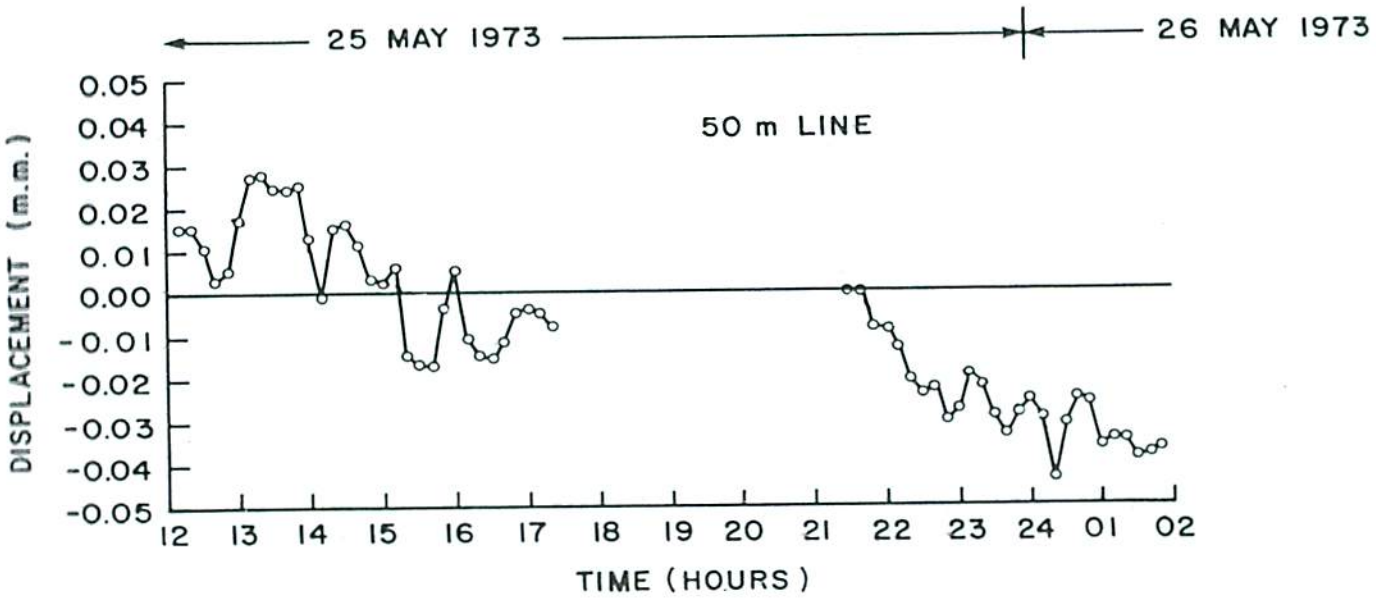

Fig. 7. Time-displacement plots for the 50 m line, May 25-26, 1973. The strain rates are $-3.0(\pm 0.6) \times 10^{-11}$ s^{-1} and $4(\pm 1) \times 10^{-11}$ s^{-1}.

because of their different lengths might be caused to bend by different amounts due to differential radiational heating. This effect, tested rigorously by repeated measurement of a single line under shaded and unshaded conditions alternately, at each end, proved to be indetectible at the 0.1 mm resolution. The results of the hexagon measurements proved irregular and this may be due to the presence and distribution of cracks, some of which are shown in Figure 3. These cracks probably form beginning in the fall when there is a rapid temperature drop and cracking sounds are frequently heard. The cracks, some of which are up to 1 cm wide, are expected to influence the surface strains depending on whether two adjacent poles straddle a crack or whether they occupy an inter-crack block. Table 1 shows the displacements occurring between poles in each line over the three time intervals taken.

A resurvey at a future date will be undertaken to clarify the nature of these strains. In general, however, the largest apparent compressive strain rate is compatible with the results obtained by the laser interferometer. For example, the line EF showed for the 14-24 May period a compressive strain rate of -2×10^{-11} s^{-1}. An adjacent line, FG, shows an extension, therefore, no direct comparisons between the hexagon and the laser line are yet possible.

TABLE 1.

Line	Length 1 May	Length 12 May	Strain rate $\times 10^{-11}$ s^{-1}	Length 24 May	Strain rate $\times 10^{-11}$ s^{-1}
EF	50.0449	50.0438	-1.9	50.0429	-2.0
EG	49.9555	49.9564	+1.6	49.9568	+1.3
EH	50.0264	50.0269	+0.9	50.0272	+0.8
EI	49.9412	49.9414	+0.4	49.9419	+0.7
EJ	49.9628	49.9624	-0.8	49.9621	-0.7
EK	50.0009	50.0003	-1.2	50.0002	-0.7
JK	50.0126	50.0133	+1.2	50.0133	+0.7
KF	49.9851	49.9849	-0.4	49.9849	-0.2
FG	50.0262	50.0264	+0.4	50.0269	+0.7
GH	49.9751	49.9754	+0.5	49.9753	+0.2
HI	50.0001	49.9999	-0.4	49.9992	-0.9
IJ	49.9324	49.9323	-0.2	49.9321	-0.3

Note: Lengths are reduced to apply at temperature of $-5^{\circ}F$ ($-20^{\circ}C$). All distances measured in catenary with central support and 15 Kg weights.

SURFACE SURVEY AND THICKNESS PROFILE

A levelling traverse was made across the short axis of the island using an Ni2 Zeiss automatic level on April 16. The resulting elevation profile is shown in Figure 9. The site for the laser experiment was selected from this on the basis of the location of the thickest ice, which under a free boundary condition would have the highest spreading rates. A 30 m SIPRE hole was drilled near the laser hut (Fig. 3). On the basis of the measured temperature profile (Fig. 10), a value for the probable thickness of the ice has been obtained. The density of the ice has been determined in the following way: let H be the thickness of ice, h be the height of the ice above water level, h' be the height above water level of the top surface when the snow has been converted into the equivalent thickness of ice, ρ_w be the density of sea water and $\overline{\rho}_i$ be the average density of the ice column.

Then for equilibrium:

$$\overline{\rho}_i = \rho_w \left(1 - \frac{h'}{(H + h' - h)} \right) \qquad (1)$$

Using values of $\rho_w = 1.0258$ g cm^{-3} (Fig. 11)
$H = 34.5 \pm 0.5$ m (Fig. 10)
$h = 3.75$ m
and $h' = 3.91$
we obtain $\overline{\rho}_i \approx 0.91$ g cm^{-3}

On the basis of this result, assuming that the average ice density has the same value everywhere, the approximate ice thickness profile across the island has been determined (Fig. 9). Figure 12 shows measured ice density and salinity values plotted against depth.

WEERTMAN CREEP

Under conditions of a free boundary the expected creep strain rate can be obtained by computing the 'effective shear stress' and then using the available stress-strain rate relationship for the appropriate temperature. According to the Weertman theory[1], the 'effective shear stress'

$$\tau = \frac{\int_0^H \int_z^H \rho_i(z)\, dz\, dz - \int_0^{\int_0^H \frac{\rho_i(z)}{\rho_w} dz} \int_0^H \rho_i(z)\, dz\, dz + \frac{1}{2}\rho_w \left[\int_0^H \frac{\rho_i(z)}{\rho_w} dz \right]^2}{\sqrt{3}\, g^{-1} A^{-1} \int_0^H A\, dz} \qquad (2)$$

for a semi-infinite slab of floating ice of thickness H and variable density $\rho_i(z)$ and modulus of plasticity A(z). g is the acceleration of gravity. If the density is assumed constant throughout, then (2) reduces to

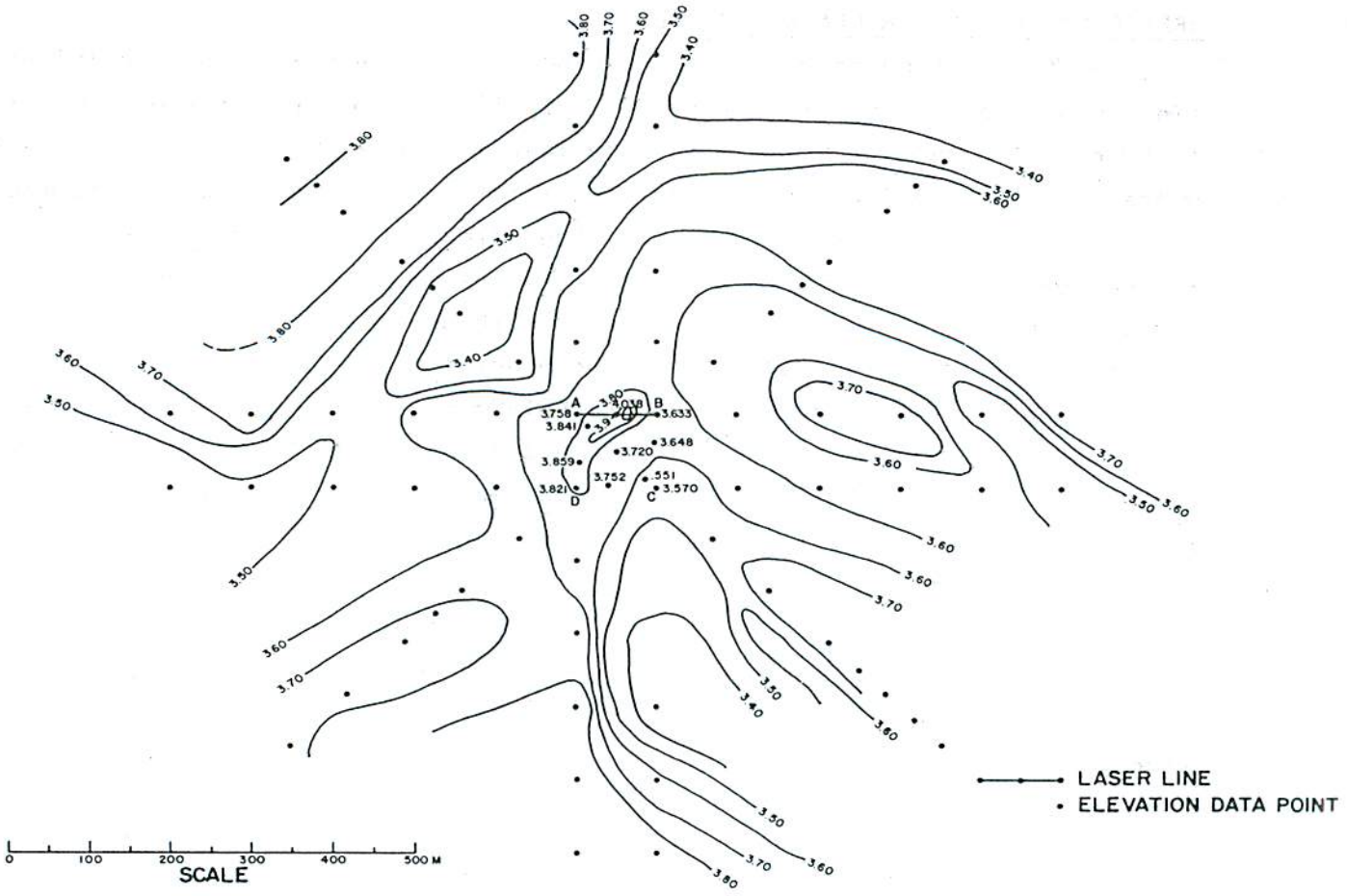

Fig. 8. Ice surface contours in the vicinity of the laser site.

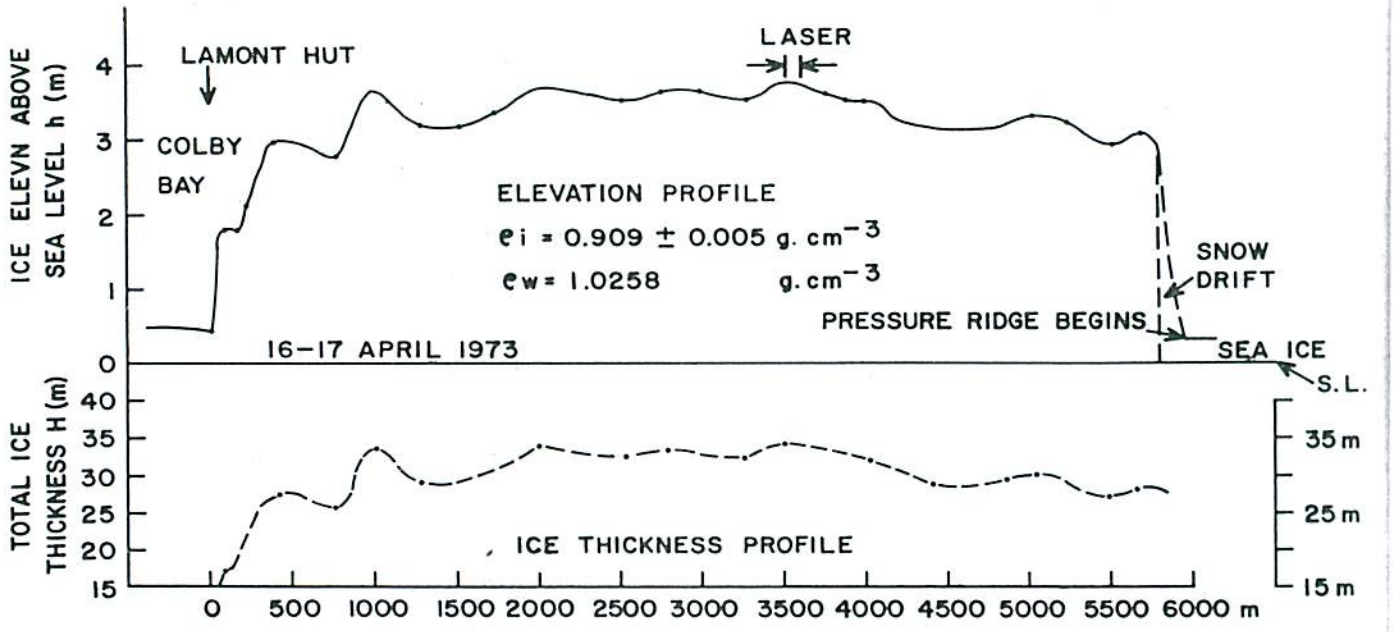

Fig. 9. Ice surface elevation profile along the minor axis of the island, approximately along reference line (Fig. 1). See also text. The ice was covered by an average of 40 cm of snow.

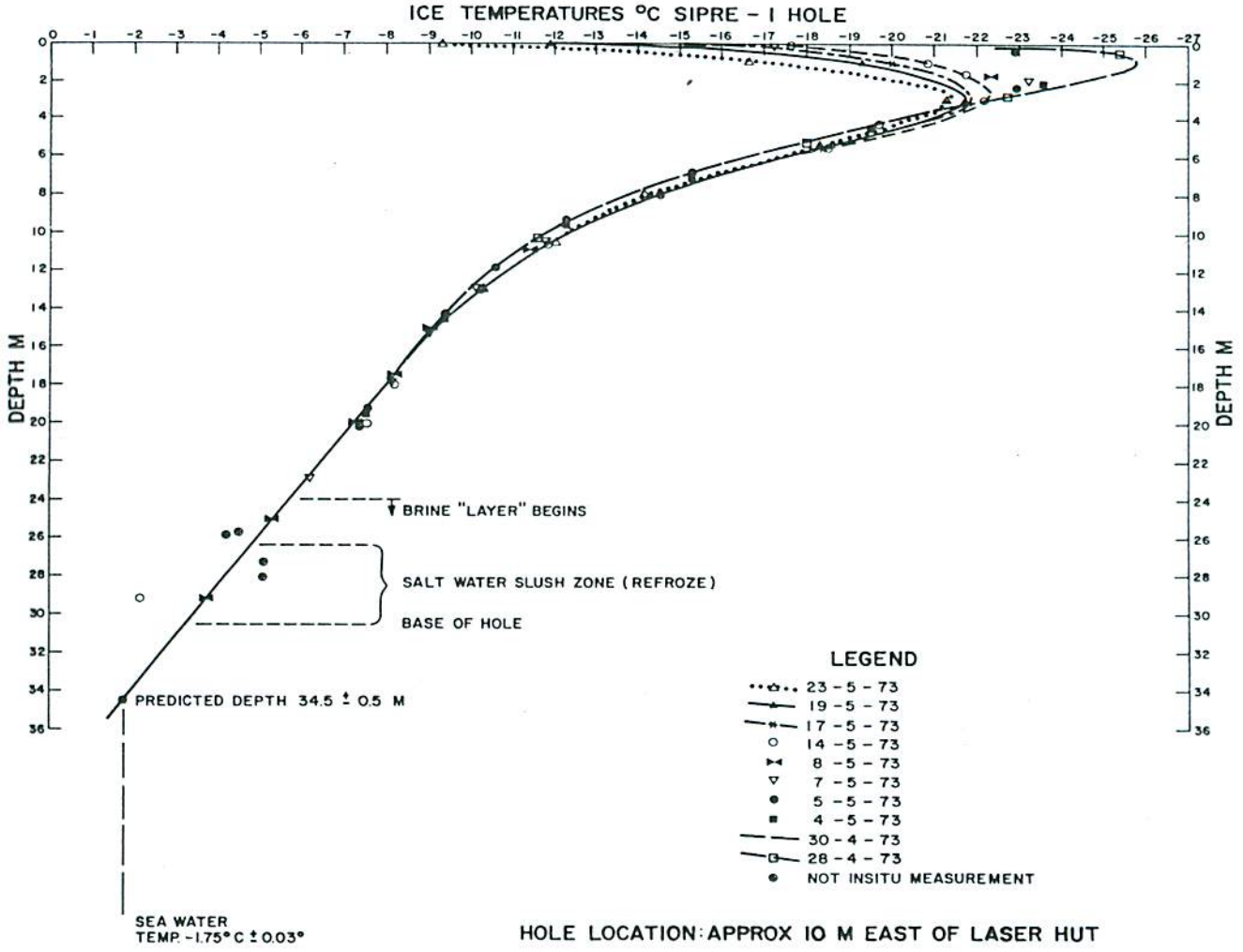

Fig. 10. Temperature - depth profile at laser site.

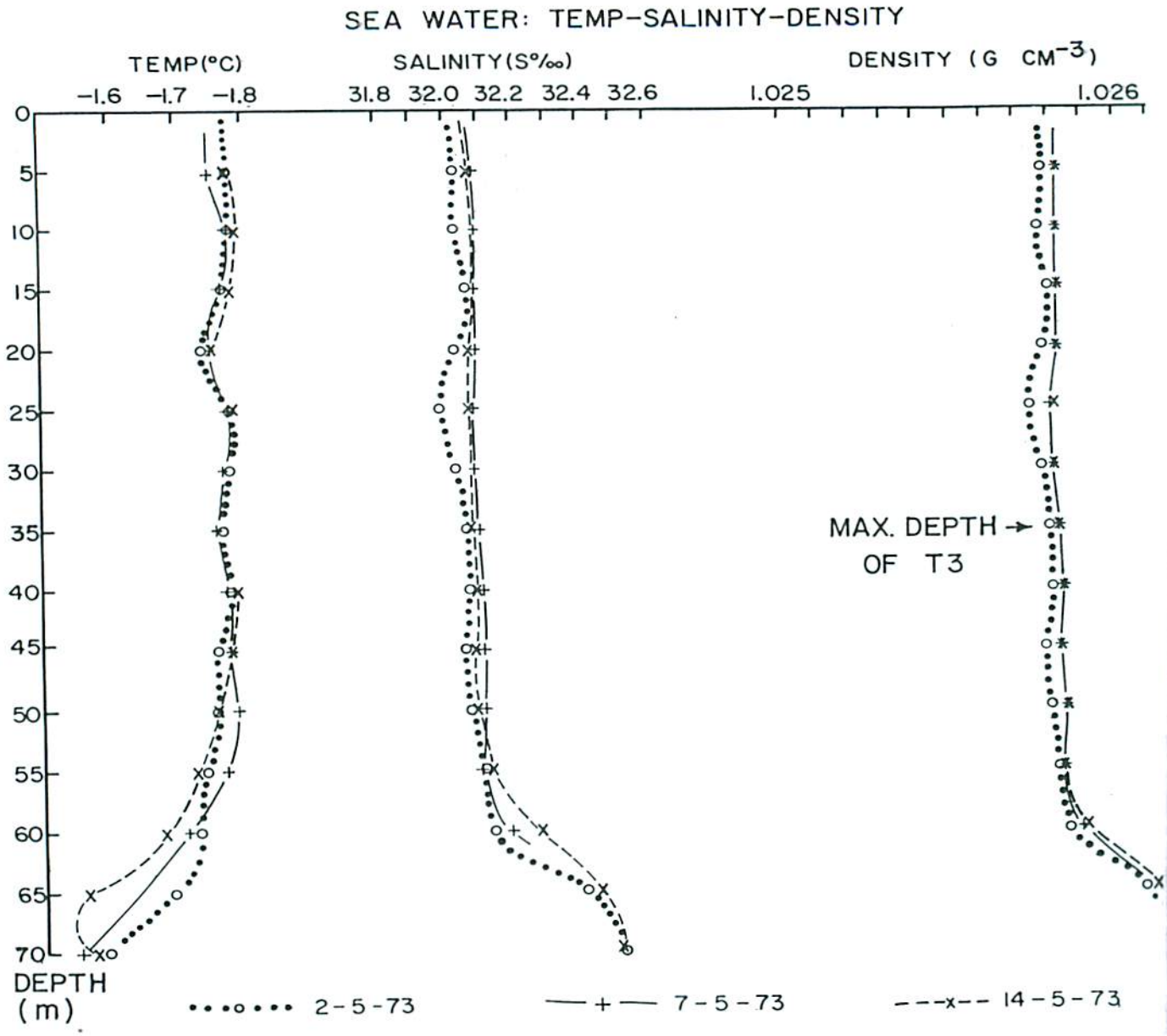

Fig. 11. Sea water temperature, salinity and density with depth in Colby Bay (Fig. 1). Data from Allen Moore, Department of Oceanography, University of Washington, Seattle.

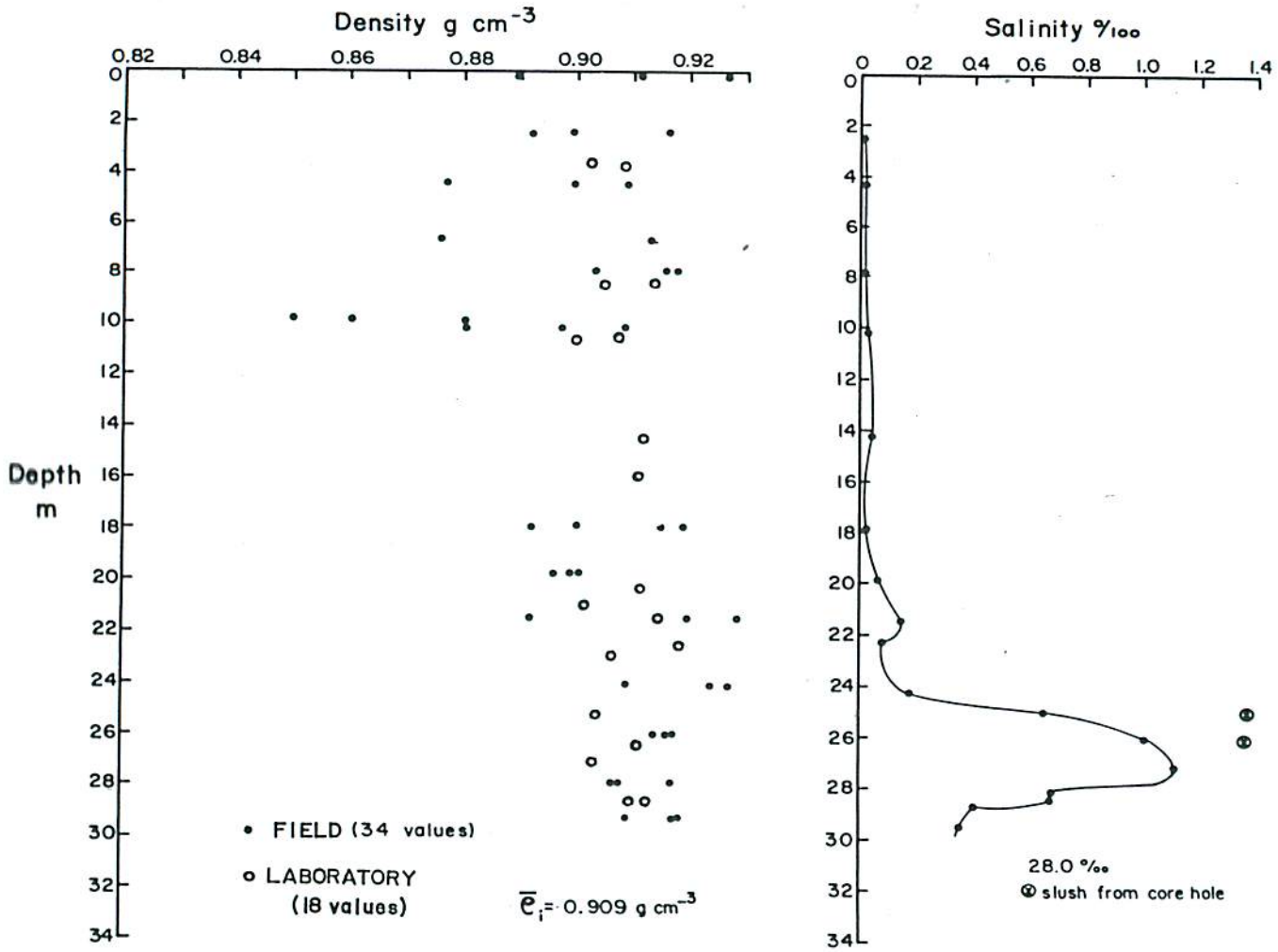

Fig. 12. Ice density and salinity variation with depth in SIPRE-1 hole.

$$\tau = \frac{\bar{\rho}_i \, g \, H h}{2\sqrt{3} \; A^{-1} \int_0^H A \, dz} \qquad (3)$$

The flow law of form $\dot{\varepsilon} = \left(\frac{\tau}{A}\right)^n$, (4)

where n is a constant, enables a value of the 'effective shear strain' rate $\dot{\varepsilon}$ to be determined. To obtain a first approximation for τ equation (3) is used. If we neglect variations in A, then for a 30 m thick ice slab where $\bar{\rho}_i = 0.91$ g cm^{-3}, h = 3.39 m; $\tau = 0.087$ bar (0.0087 MN m^{-2}). Converting to octahedral values and using the idealized flow law curves of Budd[4], we obtain an 'effective shear strain rate' of 4.9×10^{-11} s^{-1}.

For equal creep in all directions (x, y horizontal, orthogonal axes; z vertical):

$$\dot{\varepsilon}_{xx} = \dot{\varepsilon}_{yy}$$

thus $$\dot{\varepsilon}_{zz} = -2 \, \dot{\varepsilon}_{xx}$$

assuming the condition of incompressibility $\dot{\varepsilon}_{ii} = 0$. Therefore, using the expression for the 'effective shear strain rate'

$$2 \, \dot{\varepsilon}^2 = \dot{\varepsilon}_{ij} \, \dot{\varepsilon}_{ij}$$

we obtain $$\dot{\varepsilon}_{xx} = \dot{\varepsilon} / \sqrt{3} = 2.8 \times 10^{-11} \text{ s}^{-1}.$$

Where the ice is 35 m thick, the strain rate should be about 3.5×10^{-11} s^{-1}. In order to obtain a possible range for the expected strain rate, the measurements of Dorrer[5] are referred to. Dorrer measured a surface strain rate which he apparently attributed to Weertman creep. The extension rate was about 3×10^{-12} s^{-1} for a total ice thickness of 35-41 m. Hence, for a slightly thicker slab, the strain rate is a full order of magnitude less than that obtained using the data of Budd. Without entering into the validity of applying Weertman's theory, unmodified, to the results of the Ward Hunt Ice Shelf[5], we will simply specify that the expected Weertman creep rate for T 3 lies between about 3×10^{-12} s^{-1} and 3×10^{-11} s^{-1}. Thus, the strain rates would be measureable using the system that we have described. The only possibility that we may have detected these strain rates is offered by the data of the hexagonal strain net.

We conjecture that where extension has apparently occurred the poles

were located on an inter-crack block. The cracks are assumed to take up the compressive strains which allows the inter-crack blocks to creep or expand due to warming without constraint, until the cracks are closed. This implies that the expansive creep strain and the thermal expansion both overcome the compressive strain produced by the pack ice thrust. At the centre of the island this compression is expected to be more or less uniform with depth. The strain rate value of $+7 \times 10^{-12}$ s^{-1} includes thermal strain, which should also be extensive.

NEAR SURFACE TEMPERATURE CHANGES

For two poles spaced distance d apart on an inter-crack block, the spreading strain rate is about

$$\alpha \dot{\Delta T} \cdot (L/z^* + 1) \qquad (5)$$

where $\dot{\Delta T}$ is the average warming rate of the surface ice;
α is the linear coefficient of thermal expansion of the ice;
L is the length of the pole above the ice;
z^* is the depth below which daily temperature changes (averaged from one month's data) become negligible.

The value of $\dot{\Delta T}$ at the surface is about $0.2^{o}C$ per day (averaged over 1 month) (Fig. 13)

z^* is < 6 m
$\alpha \approx 50 \times 10^{-6}$ $^{o}C^{-1}$

Thus thermal strain rates could be as high as 10^{-10} s^{-1}. However, there are open cracks along the line of the laser. The average spacing of these cracks is 15 m and the width up to 1 cm, on the surface, at the time of the experiment. Thus any thermal expansion will be largely taken up by closing of the cracks. If the poles were situated in the centre of the inter-crack block, then the thermal corrections to the measured strains could be ignored. Otherwise, the thermal strain could be as high as:

$$+ \frac{10^{-10} \times 15}{100} \; s^{-1} = +1.5 \times 10^{-11} \; s^{-1}$$

EXPERIMENT TO DETECT SHORT TERM VARIATIONS IN STRAIN RATE

Figure 14 shows readings taken simultaneously from the laser display and a Lacoste and Romberg gravimeter situated in the Lamont Observatory hut located on the edge of the island. Readings were taken over a period of an hour. An average period of oscillation of the gravity meter beam is found to be

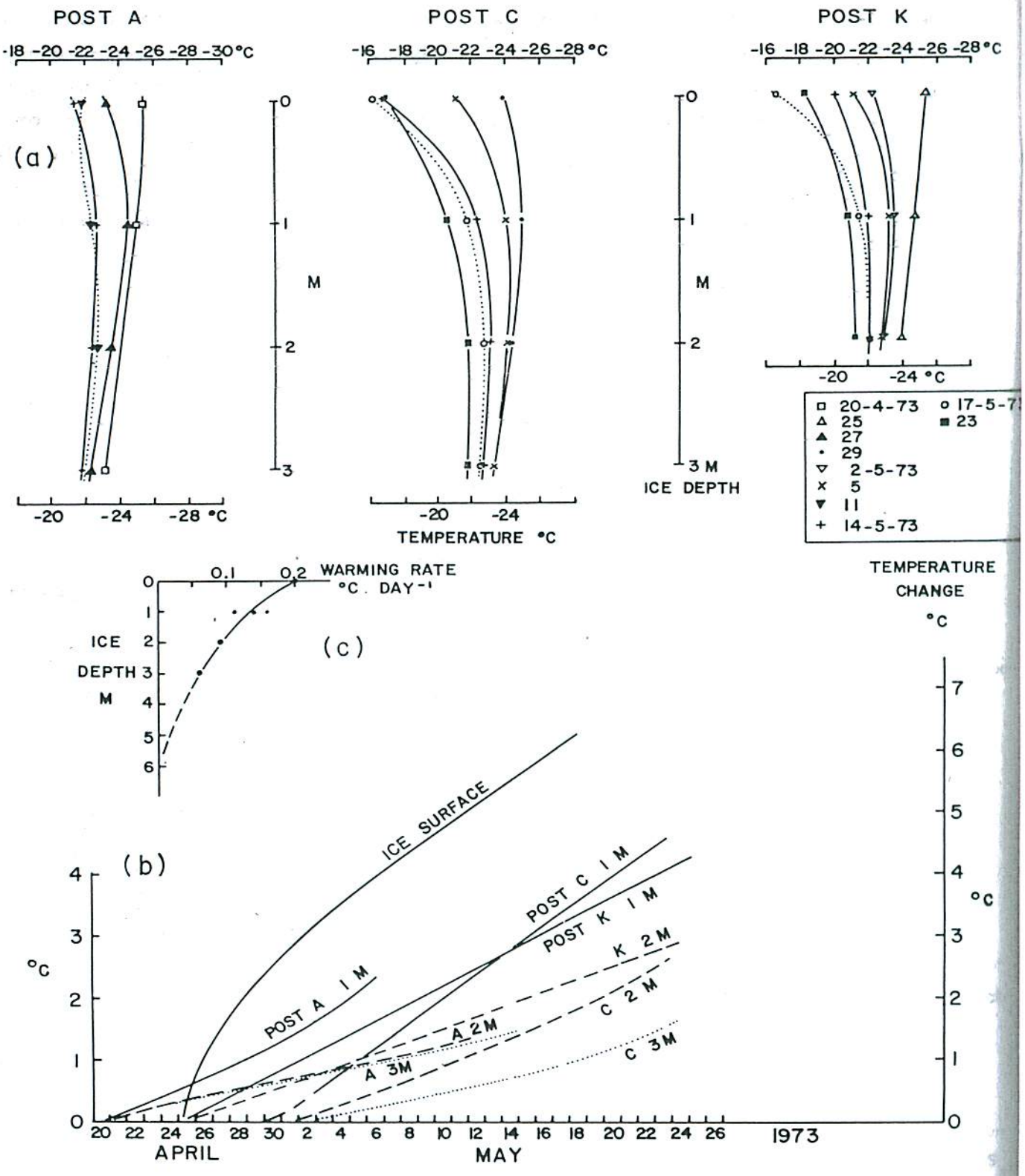

Fig. 13. (a) Temperature-depth profiles obtained from thermistor lines frozen in beside laser tubes. Curves (b) shows change of temperature with time and depth. Curve (c) shows rate of warming with depth (1 to 3 m).

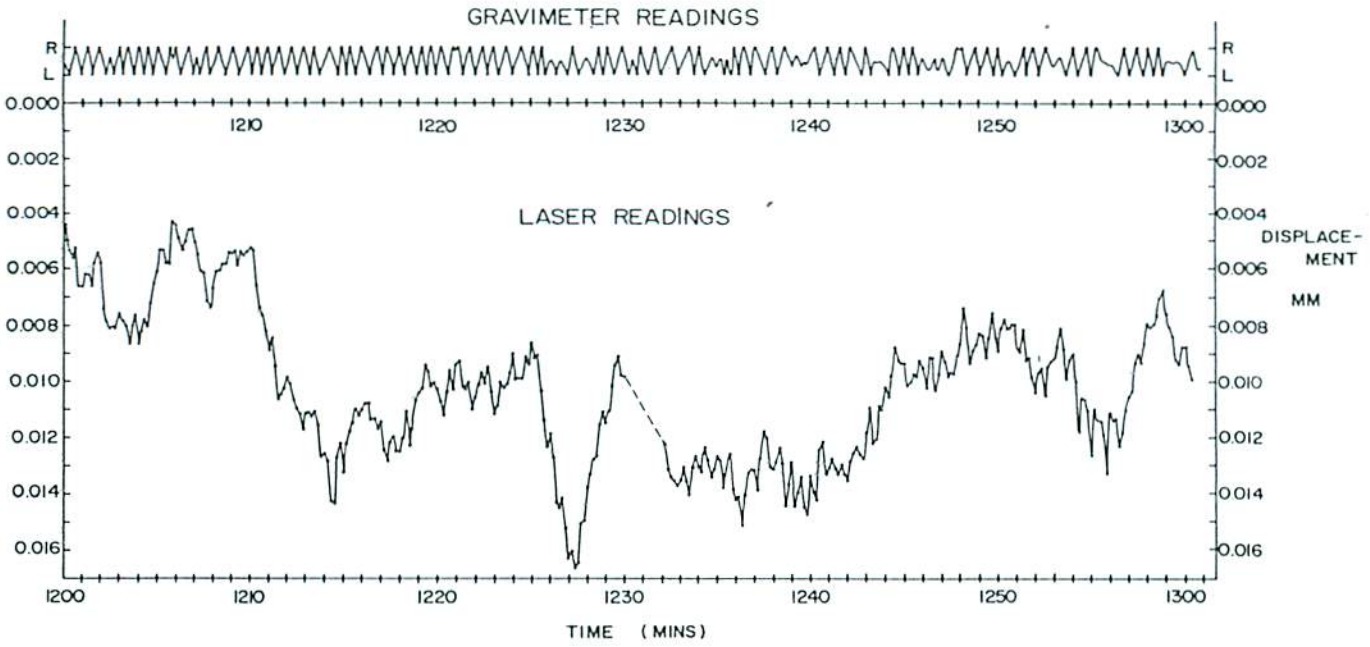

Fig. 14. Plot of gravimeter oscillations and laser display readings over a 1 hour period, May 26, 1973. R = right; L = left, stop of gravimeter scale. In most cases, the beam hit the stop; the middle of the stop reside time was taken as the turning point of the oscillation.

37 s. The natural frequencies of the island, up to the fourth mode, are less than about 11 s, thus the measured period must be the result of a characteristic ocean wave component. Crary[6] found from numerous gravity measurements made in 1952-54 that 70% of the periods fell between 33 s and 43 s, therefore, we conclude that this is a common period of oscillation for which the gravity meter is suitable for measuring. The average period of oscillation of the laser readings was found to be about 35 s with a spread from about 25-45 s. The interpretation of these data is that the island is undergoing flexural oscillations. Because there does not appear to be a phase relationship between the edge oscillations and the oscillations detected by the laser, the existence of travelling waves is expected[3].

ACKNOWLEDGEMENTS

We thank Dr. T.J. Hughes, Institute of Polar Studies, Ohio State University, and R. Weaver for participating in the project and helping to make the field work a success. Logistic support was provided by the Polar Continental Shelf Project, Department of Energy, Mines and Resources, Ottawa, Canada, the Office of Naval Research, Washington, D.C. and the Naval Arctic Research Laboratory, Pt. Barrow, Alaska. We also acknowledge the help of numerous persons on the island. M. M.Metge kindly read and improved the manuscript.

The present work was supported by the Glaciology Division, Department of the Environment. One of the Authors (A. Traetteberg) was a visiting scientist during the time that this work was being accomplished.

REFERENCES

1. Weertman, J., 1957. Deformation of floating ice shelves. Journal of Glaciology, Vol. 3, No. 21, p. 38-42.

2. Muguruma, Jiro, and Higuchi, K., 1963. Glaciological studies on Ice Island T 3. Journal of Glaciology, Vol. 4, No. 36, p. 709-730.

3. Hunkins, Kenneth, 1962. Waves on the Arctic Ocean. Journal of Geophysical Research, Vol. 67, No. 6, p. 2477-2489.

4. Budd, W.F., 1969. The dynamics of ice masses. ANARE Scientific Reports. Series A (IV) Glaciology. Publication No. 108. Department of Supply, Melbourne, Australia, 216 p.

5. Dorrer, E., 1971. Movement of the Ward Hunt Ice Shelf, Ellesmere Island, N.W.T., Canada. Journal of Glaciology, Vol. 10, No. 59, p. 211-225.

6. Crary, A.P., 1960. Geophysical studies in the Arctic Ocean. In Scientific Studies at Fletcher's Ice Island T 3, 1952-1955. Volume III. Geophysical Research Paper No. 63. Air Force Cambridge Research Centre, p. 7-30.

APPENDIX

Meteorological data for period of experiment. Temperature and humidity obtained at site Stevenson screen. Windspeed and pressure data from Lamont Geological Observatory station at main camp.

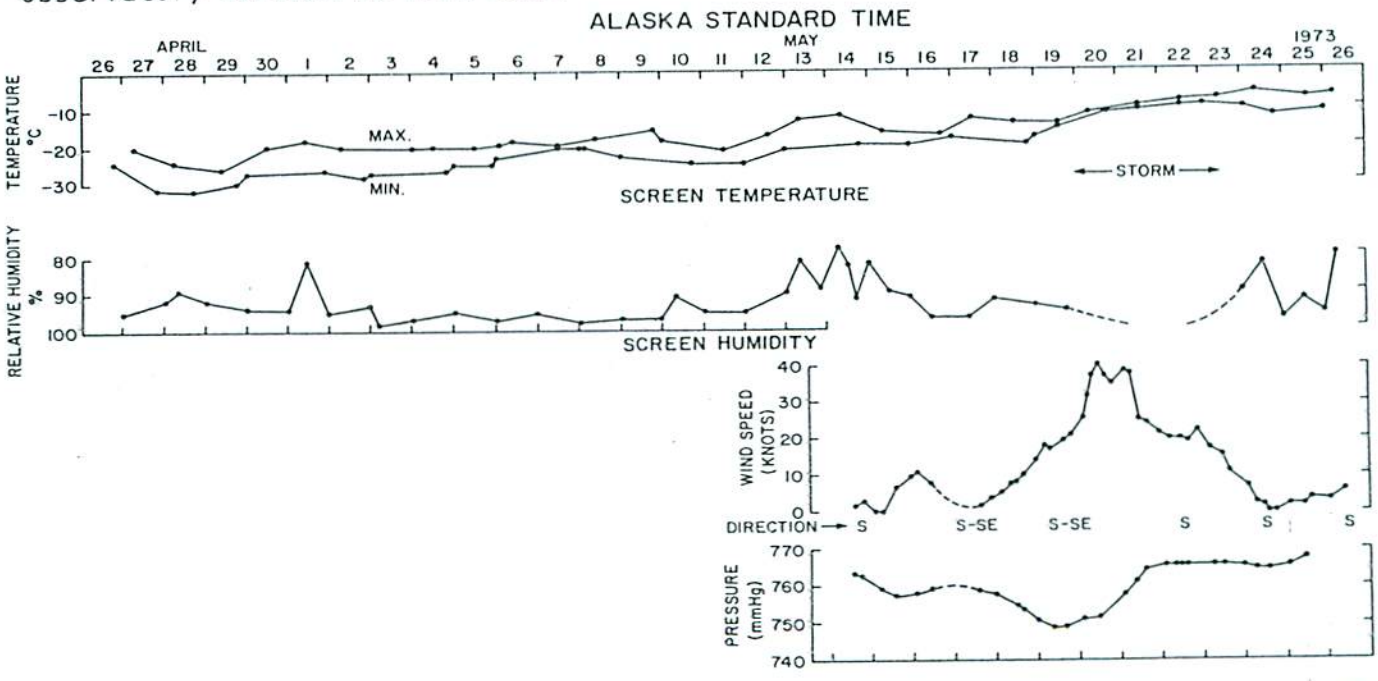

DISCUSSION

Professor R. Parmerter, AIDJEX, University of Washington, Seattle, Washington, U. S. A.:

What was the motivation behind this feasibility study? What conclusions do you hope to draw from this type of strain data?

Mr. G. Holdsworth, Glaciology Division, Inland Water Directorate, Department of the Environment, Ottawa, Canada.

First we set out to test the laser interferometer on an ice surface. Providing that our instrumentation would prove successful, our original intention was to measure the Weertman creep directly. Thus we would get a (stress, strain rate) point for ice for that particular temperature. This is in the low stress range where many of the laboratory results are in dispute. We were not able to do this because of the boundary conditions. However the strain rates that we did measure appeared to have a significance in relation to such studies as AIDJEX. They also have a bearing on the mechanical stability of the island.

Allowing for thermal and Weertman strains, the magnitude of the measured strain rates indicates compressive stresses existing in the island of at least 0.01 MN m^{-2} $^{+}50\%$ if we use stress-strain rate data of Budd. The ratio: ice island thickness/ sea-ice thickness = 10, therefore the compressive stresses in the sea-ice could have been at least 0.1 MN m^{-2} (1 x 10^6 dynes.cm^{-2})$\pm$ 50%. However these values do not apply at the time of the observed ridging shown in Fig. 2 of our paper. At that time the stresses could very well have been higher. During this period, the motion of the gravimeter became very irratic (Alan Gill, personal communication) implying a jerky application of stress to the island. Although there is a different model involved here this behaviour is consistent with Parmerter and Coon's kinematic ridge model and with the general observation that ridging occurs in "fits and starts".

Professor R. Parmerter:

The stress value given is equivalent to 3 x 10^8 dynes. cm^{-1} (force per unit length, integrated through the sea ice sheet). This number is consistent with the forces required to ridge strong 3M ice, as calculated from the model proposed in the paper "On the mechanics of pressure ridge formation in sea ice", Proc. 5th Offshore Technology Conference, Parmerter and Coon, 1973. You mentioned that ridging had occurred around the island. This is the only example I know of where the ice pressure close to the condition of ridging has been determined, and it is very gratifying to learn that the value required by our model seems to be of the right order.